UNDERSTANDING THE INTERFACIAL INTERACTIONS IN SILICA REINFORCED POLYPROPYLENE NANOCOMPOSITES

D. Pedrazzoli[a,b*], A. Pegoretti[a], K. Kalaitzidou[b,c]

[a]*Department of Industrial Engineering, University of Trento, Via Mesiano 77, 38123 Trento (Italy)*
[b]*G. W. Woodruff School of Mechanical Engineering, Georgia Institute of Technology, 801 Ferst Drive Atlanta GA 30336 (USA)*
[c]*School of Materials Science and Engineering, Georgia Institute of Technology, 771 Ferst Drive Atlanta GA 30322 (USA)*
**d.pedrazzoli@ing.unitn.it*

Keywords: Silica, Interfacial interactions, Interphase, Crystallization.

Abstract
In this study, polypropylene (PP) matrices containing various types and amounts of silica nanoparticles were prepared by melt compounding and injection molding. Both non-functionalized and dimethyldichlorosilane-functionalized silica nanoparticles were used. Three-component PP matrices were also prepared by including selected formulations of both Poly(propylene-g-maleic anhydride) copolymer (PPgMA) and different types of silica. Both silica types were found to provide a stiffening effect and enhance the viscoelastic behavior of PP, as determined by quasi-static tensile tests and dynamic mechanical analyses (DMA). The properties of the polymer/nanofiller interphase were investigated by modulated differential scanning calorimetry (DSC) and DMA. A strong correlation between the glass transition temperature (T_g) and the tensile elastic modulus indicated the presence of secondary reinforcing mechanisms in silica PP nanocomposites.

1. Introduction

A novel class of materials, namely the polymer nanocomposites, has recently shown new and novel properties thanks to the addition of nanostructured materials such as fumed silica, carbon nanotubes and graphite nanoplatelets. The advantage of nanocomposites over the traditional microcomposites is that thanks to their extremely high surface area, a dramatic improvement of the mechanical properties, thermal behaviour, gas barrier properties, thermal and electrical conductivity can be achieved at very low filler contents (less than 5 wt%) [1, 2]. However, the unique properties of the nano-reinforcements cannot be fully exploited in nanocomposites due to agglomeration and weak interface, resulting in reduced stress transfer [3].
The recent literature highlights the need of considering various experimentally observed filler characteristics such as aspect ratio, agglomerate size and presence and properties of interphase in order to develop better design tools to fabricate multifunctional polymer composites [4]. In particular, it is of great interest to understand how nano-scale interfacial interactions affect the macro-scale properties in polymer nanocomposites. Present research has been mainly focused on the understanding of the mechanisms involved in the polymer chain dynamics upon nanofiller modification. However, very few studies have been dedicated to the modeling of the relationships between the macroscopic mechanical properties of nanocomposites and their

interfacial strengths. Therefore, the main aim of this study is to provide a better understanding on the role of interfacial interactions in affecting the physical characteristics of the polypropylene (PP) matrix and in turn enhancing the macroscopic mechanical performances of PP nanocomposites. The study of the thermo-mechanical properties of the polymeric matrix upon addition of nanofiller is used to reveal the relationships among interfacial interactions, tensile properties and viscoelastic behavior in silica polypropylene composites. In order to generate different interfacial interactions, both untreated and silane-treated silica particles are used to produce the materials under investigation.

2. Experimental section

2.1 Materials and samples preparation

The matrix of the nanocomposites used in this work was an isotactic homopolymer polypropylene (MFI at 190 °C and 2.16 kg = 6.9 g/10', density = 0.904 g/cm^3) produced by Polychim Industrie S.A.S. (LOON-PLAGE, France) with the commercial code PPH-B-10-FB. FUSABOND® P M-613-05 maleic anhydride modified polypropylene (PPgMA) (MFI at 190 °C and 2.16 kg = 106.8 g/10', density = 0.903 g/cm^3, maleic anhydride content = 0.35-0.70 wt%), was supplied by DuPont™ de Nemours (Geneva, Switzerland).
Both untreated and surface treated fumed silica nanoparticles were supplied by Evonik Industries AG (Hanau, Germany). Untreated nanoparticles (Aerosil® A380) had an average primary particle size of 7 nm and a specific surface area of 321±3 m^2/g, as determined by BET analysis [5]. Dimethyldichlorosilane functionalized silica nanoparticles (Aerosil® R974) were characterized by an average primary particle size of 12 nm and a BET specific surface area of 124±1 m^2/g.
Nanocomposite samples were produced by melt mixing and injection molding. A vertical, co-rotating, bench-top twin-screw micro-extruder (DSM Micro 15cm^3 Compounder) connected to a micro-injection molding unit (DSM) were used in order to get dogbone specimens. The compound was mixed for 3 min, at 190 °C and a screw speed of 250 rpm. The temperature of the mold was 80 °C, while the injection molding pressure was about 800 KPa. Ternary nanocomposites were prepared by adding 5 wt% of PPgMA as a compatibilizer to the systems containing 5 wt% of silica.
Composites were designated indicating the matrix, the compatibilizer (if any) with its content and the filler type with its amount. For instance, a sample filled with 5 wt% of PPgMA and 5 wt% of Aerosil® A380 was indicated as PP-PPgMA-5-A380-5.

2.2 Experimental techniques
2.2.1 Morphology characterization

Fracture surfaces of nanocomposite samples were observed at various magnifications by using a Phenom G2 Pro (Phenom-World BV., Eindhoven, The Netherlands) bench-top scanning electron microscope (SEM), at an acceleration voltage of 5 kV. Prior to the SEM observations, a thin gold coating was applied onto the surface by plasma sputtering in order to minimize the charging effects.

2.2.2 Thermal characterization

Standard differential scanning calorimetry (DSC) and modulated DSC tests were carried out by a DSC Q2000 (TA Instruments, New Castle, Delaware, USA) under a constant nitrogen flow of 50 ml/min on specimens of about 5-8 mg. The samples were heated up from the

equilibrated temperature of 0 °C to 200 °C at a rate of 5 °C/min with subsequent crystallization test down to 0 °C, setting a cooling rate of 5 °C/min. During heating and cooling a modulation of ± 1 °C every 60 s was set in order to decompose the total heat flow signal into reversing and non-reversing information.

2.2.3 Mechanical testing

Uniaxial ramp tensile tests were performed according to ASTM D638 with an Instron model 33R 4466 (Norwood, USA) tensile tester equipped with a 500 N load cell, on samples consisting of at least five dogbone specimens. Tests were carried out at a crosshead speed of 5 mm/min. Axial strain was recorded by using a resistance extensometer Instron® model 2630-101 with a gauge length of 10 mm. The elastic modulus was measured as secant modulus between longitudinal deformation levels of 0.05 % and 0.25 %. Dynamic mechanical analyses (DMA) were carried out at a DMA Q800 (TA Instruments, New Castle, Delaware, USA) testing machine over a temperature range between -20 °C and 160 °C, imposing a heating rate of 5 °C/min and a frequency of 1 Hz. A preload of 0.2 MPa and a maximum strain of 0.05 % were imposed on rectangular samples 25 mm long, 3.30 mm wide and 3.27 mm thick. The most important viscoelastic functions (*E', E'', tan(δ)*) were recorded at different temperatures.

3. Results and discussion

3.1 Tensile mechanical properties and viscoelastic properties

The tensile elastic modulus and the glass transition temperature, evaluated by DMA analysis as the temperature correspondent to the tan(δ) peak, were found to follow a similar trend when considered as a function of the filler content (Figure 1(a-b)). In particular, modulus and T_g of the composites based on silica A380 increase with filler content up to ~1 wt%, reaching a plateau at filler loadings between 1 and 3 and continue increasing at higher filler amounts. This non-monotonical trend indicate the presence of two competing effects, specifically the stiffening effect given by high modulus silica particles (E ~ 70 GPa) and the formation of silica aggregated because of poor dispersion within the matrix. On the other hand, PP-R974 composites manifested a monotonical trend characterized by a greater increase of the quantities at low filler content, reaching almost a plateau at higher filler amounts.

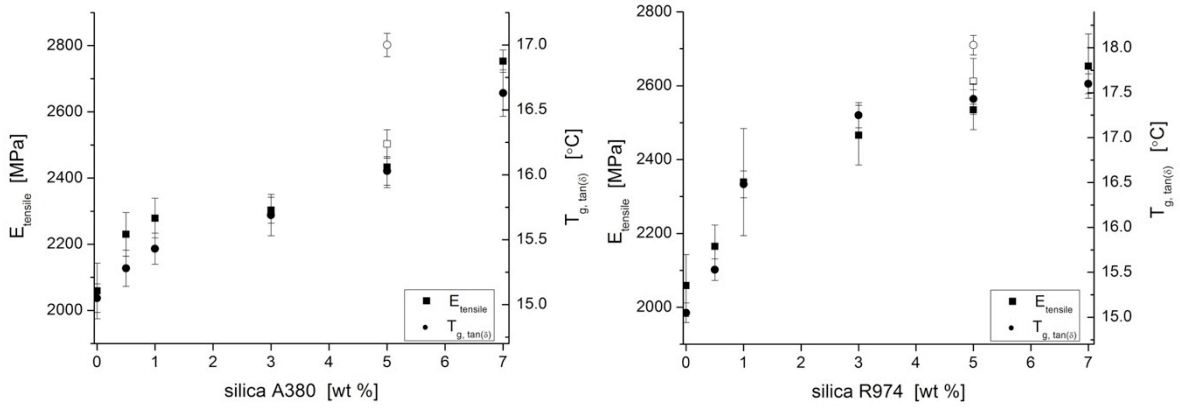

(a) (b)

Figure 1. Tensile elastic modulus and T_g obtained from DMA of (a) PP-A380 and (b) PP-R974 composites as a function of the filler content. The compatibilized samples (i.e. PP-PPgMA-5-A380-5 and PP-PPgMA-5-R974-5) are represented by open point in their correspondent plots.

The strong correlation between the tensile modulus and T_g, which is related to the immobilized fraction of the polymer chains in the amorphous region, motivated further investigation on the polymer/filler interfacial interaction.

3.2 Relationships between interfacial interactions and the tensile and viscoelastic properties

Unlike fiber-reinforced composites, the interfacial interactions in particulate-filled composites is hard to measure directly. In order to overcome this technical issue, Pukanszky [6] developed a model expressing the ratio of the yield stress of the nanocomposites to that of the neat polymer ($\sigma_{y,c}$ / $\sigma_{y,m}$) as a function of the filler volume fraction ϕ:

$$\frac{\sigma_{y,c}}{\sigma_{y,m}} = \frac{1-\phi}{1+2.5\phi}\exp(B_P\phi) \qquad (1)$$

where the fraction [(1-ϕ)/(1+2.5ϕ)] takes into consideration the decrease of the effective load-bearing cross-section, while the exponential represents all other effects resulting in an increase of the yield stress [7]. Specifically, the parameter B_P accounts for the interface and interphase properties and larger B_P values correspond to higher interfacial adhesion [8]:

$$B_P = (1+\tau\,\rho_f\,S_f)\ln\left({}^{\sigma_{y,i}}/_{\sigma_{y,m}}\right) \qquad (2)$$

where τ is the thickness of the interphase, while the quantities ρ_f, S_f and $\sigma_{y,i}$ represent the density of the filler, the specific surface area of the filler and the yield stress of the interphase, respectively. Because of obvious technical difficulties in providing reliable values of the thickness and yield stress of the interphase, the parameter B_P can be extrapolated from the experimental data according to Eq. (1):

$$B_P = \frac{1}{\phi}\,ln\left(\frac{\sigma_{y,c}}{\sigma_{y,m}}\,\frac{1+2.5\phi}{1-\phi}\right) \qquad (3)$$

On the other hand, Sumita et al [9] proposed a model to express the ratio of the loss modulus of the nanocomposites to that of the neat polymer (E''_c/E''_m) as a function of the effective volume fraction of the dispersed phase (ϕ_e), which is represented by the volume of filler (ϕ) plus that of the 'constrained matrix' associated with the interface :

$$\frac{E''_c}{E''_m} = (1-\phi_e)^{-1} = (1-\phi\,B_s)^{-1} \qquad (4)$$

where the parameter B_S describes the relative value of the effective volume per single particle. In order to investigate the relationships between interfacial interactions and the tensile and viscoelastic properties, the parameters B_P and B_S are plotted as a function of the filler volume fraction ϕ for PP-A380 and PP-R974 samples in Figure 2(a-b). For both samples, B_P and B_S increase up to a threshold value ~0.005-0.010 vol% (correspondent to ~1-3 wt%) and decrease at higher volume fractions. This trend indicates that the polymer/filler interfacial adhesion is enhanced up to the threshold value, while the higher concentration of aggregates at greater filler contents leads to a significant decrease in the average specific surface area of silica particles, resulting in a decrease of the B parameters [7]. Specifically, when passing the

threshold filler value, the value of ϕ_e increases less rapidly with further addition of particles, indicating that the thickness of the physically absorbed PP layer on the surface of the silica particles is limited due to the agglomeration [8].

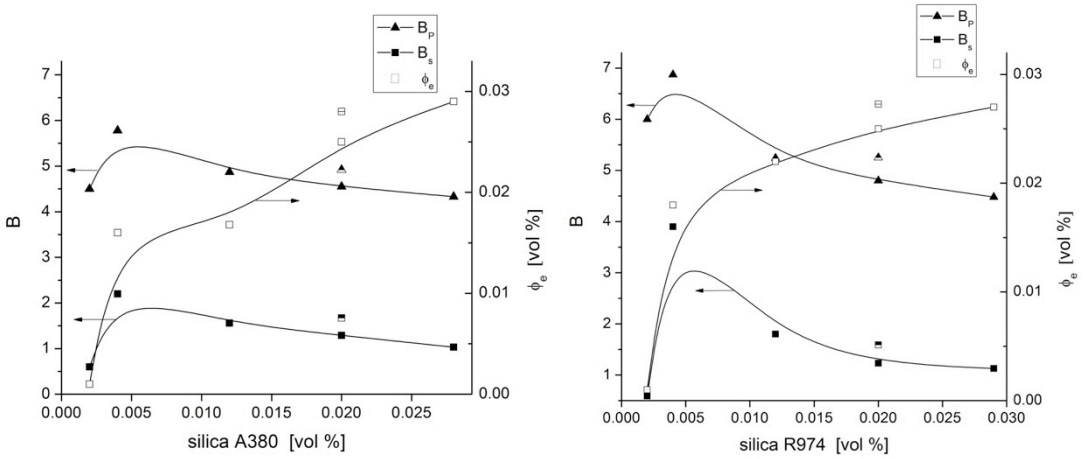

Figure 2. Plot of the *B* parameters and of the effective volume fraction of the dispersed phase (ϕ_e) as a function of the filler volume content for (a) PP-A380 and (b) PP-R974 composites. Half full points denote data related to the PP-PPgMA-5-silica-5 samples.

3.3 Complex constrained phase at the filler surface

The recent literature reports evidence of the formation of a complex polymer phase constrained on the filler surface. In particular, the model proposed by Karevan and Kalaitzidou for particle-filled semicrystalline polymers considers as constrained phase *(C)* the crystalline phase *(χ)* and part of the amorphous phase that is immobilized not only at the crystal surface but also on the filler surface *(C-χ)* [10]. The rest of the amorphous phase is considered as the mobile phase (Table 1). In particular, the degree of crystallinity was calculated by taking the weight fraction of PP in the composite into account, according to the following equation:

$$\chi_{\%} = \frac{\Delta H}{\Delta H_m^* \left(1 - {wt_{\%}}/{100}\right)} 100 \qquad (5)$$

where ΔHm^* is the melting enthalpy of 100% crystalline isotactic PP equal to 209 J/g [11].

Sample	χ [%]	tan(δ) $_{Tg}$	C [%]	(C-χ) [%]	Induction time [min]
PP	41.8 ± 0.2	0.0789 ± 0.0010	41.8	0.0	3.70 ± 0.05
PP-A380-0.5	41.4 ± 0.3	0.0762 ± 0.0006	43.4	2.0 ± 0.3	3.85 ± 0.07
PP-A380-1	40.0 ± 0.2	0.0747 ± 0.0009	44.3	4.3 ± 0.2	3.96 ± 0.04
PP-A380-3	38.6± 0.3	0.0732 ± 0.0010	45.2	6.6 ± 0.3	4.14 ± 0.06
PP-A380-5	38.5 ± 0.2	0.0717 ± 0.0008	46.1	7.6 ± 0.2	4.21 ± 0.05
PP-A380-7	34.8 ± 0.3	0.0657 ± 0.0007	49.8	15.0 ± 0.3	4.28 ± 0.05
PP-R974-0.5	41.8± 0.2	0.0743 ± 0.0010	44.5	2.7 ± 0.2	3.74 ± 0.06
PP-R974-1	40.6 ± 0.3	0.0732 ± 0.0009	45.2	4.6 ± 0.3	3.78 ± 0.06
PP-R974-3	39.2 ± 0.4	0.0715 ± 0.0006	46.2	7.1 ± 0.4	3.98 ± 0.04
PP-R974-5	37.9 ± 0.2	0.0700± 0.0009	47.2	9.2 ± 0.2	4.11 ± 0.05
PP-R974-7	34.7 ± 0.4	0.0663 ± 0.0008	49.5	14.8 ± 0.4	4.23 ± 0.07
PP-PPgMA-5-A380-5	38.0 ± 0.2	0.0654 ± 0.0007	50.0	12.0 ± 0.2	4.58 ± 0.04
PP-PPgMA-5-R974-5	38.4 ± 0.3	0.0640 ± 0.0009	50.9	12.5 ± 0.3	4.41 ± 0.06

Table 1: Crystallization and viscoelastic properties of the silica nanocomposites.

The presence of an immobilized amorphous phase at the filler surface is also evidenced in the viscoelastic behavior. In particular, the *tan(δ)* peak value, evaluated at T_g, decreases and shifts towards higher temperatures upon filler incorporation (Table 1 and Figure 1). This trend indicates that the filler decreases the viscous and improves the elastic behavior of PP by pinning the polymer chains and forming an immobilized region.
The non-isothermal crystallization behavior, as studied by MDSC, showed that incorporation of increasing amounts of filler results in a progressive increase of the onset crystallization temperature (i.e. characterizing the beginning of the crystallization), indicating a nucleation effect. Therefore, the crystallization induction time (Δt_i), defined as the time difference between onset and endset time of the crystallization, was found to increase with the filler content (Table 1), evidencing that the polymer chain have longer time to re-arrange and forming more perfect and / or thicker crystals [12].
Considering also the nucleation effect produced by silica fillers (i.e. more surfaces are available for nucleation of new crystals), the observed crystallization behavior indicates
that a transcrystalline phase forms on the filler surface during crystallization. Therefore, the immobilized constrained phase consists of the immobilized amorphous and the immobilized transcrystalline phase.

3.4 Morphology characterization

SEM micrographs of fracture surfaces for PP nanocomposites loaded with 5 wt% silica are shown in Figure 4(a-b). Isodimensional silica aggregates appear distributed quite homogeneously within the matrix in PP-A380-5 nanocomposite (Figure 4a). On the other hand, the incorporation of surface-treated silica seems to promote a better dispersion of the filler, as the size of aggregates is markedly lower (Figure 4b). Moreover, the smaller aggregate dimensions observed in PP-R974-5 composites can substantiate the better tensile and viscoelastic mechanical properties when compared to PP-A380-5 sample (Figure 1).

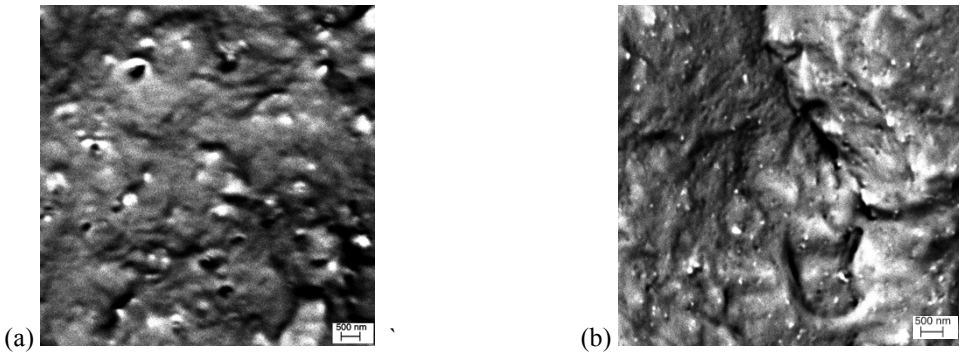

Figure 4. SEM micrographs of fracture surfaces of (a) PP-A380-5, (b) PP-R974-5 (c) PP-A380-7 and (d) PP-R974-7.

4. Conclusions

This study focused on understanding the interfacial interactions occurring between nanosilica and polypropylene and their effect on the physical and macroscopic properties of PP-silica nanocomposites. A significant correlation between the tensile modulus, glass transition temperature and the amount of constrained phase, as assessed through tensile and DMA analyses, revealed the presence of a secondary reinforcing mechanisms, which, concurrently to the primary stiffening effect of the high modulus filler, contributes to the enhancement of the nanocomposites bulk properties. Crystallization experiments evidenced the existence of a

transcrystalline region generating thanks to the nucleating ability of the filler, while DMA experiments were also used to confirm the presence of an immobilized amorphous phase at the filler surface. A complex constrained phase, responsible for providing a secondary reinforcing mechanism, was thus modeled as immobilized amorphous and transcrystalline regions located at the filler surface.

References

[1] F. Hussain. Review article: Polymer-matrix Nanocomposites, Processing, Manufacturing, and Application: An Overview. *Journal of Composite Materials*, 40: 1511-1575, 2006.

[2] D. Pedrazzoli, A. Dorigato and A. Pegoretti. Monitoring the mechanical behaviour of electrically conductive polymer nanocomposites under ramp and creep conditions. *Journal of Nanoscience and Nanotechnology*, 12: 4093-4102, 2012.

[3] R. K. Duncan, X. G. Chen, J. B. Bult, L. C. Brinson and L. S. Schadler. Measurement of the critical aspect ratio and interfacial shear strength in MWNT/polymer composites. *Composites Science and Technology*, 70: 599-605, 2010.

[4] M. A. Bhuiyan, R. V. Pucha, J. Worthy, M. Karevan and K. Kalaitzidou. Defining the lower and upper limit of the effective modulus of CNT/polypropylene composites through integration of modeling and experiments. *Composite Structures*, 95: 80-87, 2013.

[5] A. Dorigato, A. Pegoretti and A. Penati. Linear low-density polyethylene – silica micro- and nanocomposites: dynamic rheological measurements and modeling. *eXPRESS Polymer Letters*, 4: 115-129, 2010.

[6] B. Pukanszky, B. Turcsanyi and F. Tudos. *Effect of interfacial interaction on the tensile yield stress of polymer composites in Interfaces in Polymer, Ceramic and Metal Matrix Composites*. Elsevier, New York, 1988.

[7] N. Aït Hocine, P. Médéric and T. Aubry. Mechanical properties of polyamide-12 layered silicate nanocomposites and their relations with structure. *Polymer Testing,* 27: 330-339, 2008.

[8] M. Z. Rong, M. Q. Zhang, S. L. Pan, B. Lehmann and K. Friedrich. Analysis of the interfacial interactions in polypropylene/silica nanocomposites. *Polymer International*, 53: 176-183, 2004.

[9] M. Sumita, K. M. Tsukihi, K. Ishikawa. Dynamic Mechanical Properties of Polypropylene Composites Filled with Ultrafine Particles. *Journal of Applied Polymer Science*, 29: 1523-1530, 1984.

[10] M. Karevan and K. Kalaitzidou. Formation of a complex constrained region at the graphite nanoplatelets-polyamide 12 interface. *Polymer*, 54: 3691-3698, 2013.

[11] E. James. *Polymer data handbook*. Oxford University Press, New York, 1999.

[12] W. A. Y. Yusoff, K. D. Dotchev and D. T. Pham. Deterioration of polyamide powder properties in the laser sintering process. In *Proceedings of the Institution of Mechanical Engineers, Part C: Journal of Mechanical Engineering Science*, volume 222, pages 2163-2176, 2008.